Available online at www.sciencedirect.com
SCIENCE DIRECT®
Solid State Ionics 158 (2003) 167–175
SOLID STATE IONICS
www.elsevier.com/locate/ssi

Electronic structure of Ag_2S, band calculation and photoelectron spectroscopy

S. Kashida[a,*], N. Watanabe[b], T. Hasegawa[b], H. Iida[b], M. Mori[c], S. Savrasov[d]

[a] Department of Environmental Science, Niigata University, Ikarashi 8050, Niigata 950-2181, Japan
[b] Graduate School of Science and Technology, Niigata University, Ikarashi 8050, Niigata 950-2181, Japan
[c] School of Informatics and Sciences, Nagoya University, Furo-cho, Chikusa-ku, Nagoya 464-8601, Japan
[d] Department of Physics and Astronomy, Rutgers University, 136 Frelinghuysen Rd., Piscataway, NJ 08854-8019, USA

Received 8 April 2002; received in revised form 12 September 2002; accepted 30 September 2002

Abstract

The electronic structure of the silver chalcogenide compound Ag_2S has been investigated, experimentally using photoelectron spectroscopy, and theoretically using the full-potential LMTO calculation. The photoemission data taken using a synchrotron photon source is compared with the calculated valence density of states (DOS). The band structure is also calculated for the high-temperature cubic disorder phase. For that sake, a hypothetical ordered structure model is utilized instead of the disorder structure. From the hitherto reported crystallographic data and the calculated total energies, microscopic mechanisms of the phase transition and superionic conduction are discussed.

PACS: 71.15.La; 79.60.−i; 66.30.Dn
Keywords: Superionic conductor; LMTO; Photoemission; Phase transition

1. Introduction

Silver chalcogenide compound, Ag_2S, known as a coinage mineral undergoes a structural phase transition. Above 453 K, Ag_2S has a cubic structure called argentite (α-Ag_2S). At room temperature, Ag_2S changes to a monoclinic structure called acanthite, space group $P2_1/c$ and $Z=4$ (β-Ag_2S [1,2]). Both the α and β phases have in common a body-centered cubic arrangement of sulfur atoms. In the α-phase, silver atoms are randomly distributed over the interstices of the sulfur lattice [3]. A single crystal neutron scattering experiment [4] has shown that silver atoms have liquid-like distribution along the $<100>_c$ channel. Ag_2Se also belongs to the bcc silver chalcogen family. The crystallographic data of Ag_2Se is still contradictory. From powder X-ray data, Wiegers [5] proposed an orthorhombic structure with space group $P2_12_12_1$. According to the recent electron diffraction study by De Ridder and Amelinckx [6], however, two different types coexist, one is monoclinic and the other is triclinic (pseudoorthorhombic, with cell dimensions similar to those reported in the X-ray study [5]). Above 406 K, Ag_2Se transforms also to the bcc (α)-

* Corresponding author. Fax: +81-25-262-6131.
E-mail address: kashida@sc.niigata-u.ac.jp (S. Kashida).

0167-2738/02/$ - see front matter © 2002 Elsevier Science B.V. All rights reserved.
PII: S0167-2738(02)00768-3

phase. The ion dynamics in the silver chalcogenide compounds have extensively been studied, using diffuse X-ray and neutron scatterings [7–9], and molecular dynamics calculations [10,11].

The electrical property of Ag_2S and Ag_2Se has been studied by several researchers, as a function of Ag concentration [12,13]. β-Ag_2S behaves like a semiconductor ($d\sigma/dT>0$, with activation energy of 1.3 eV). Across the β–α phase transition of Ag_2S, the ionic conductivity increases nearly two orders of magnitude, while the electronic conductivity increases nearly three orders of magnitude [12,13]. α-Ag_2S behaves like a metal ($d\sigma/dT<0$). Thus, the β–α transition of Ag_2S has a character of semiconductor–metal transition. β-Ag_2Se also behaves like a semiconductor and α-Ag_2Se like a metal [13].

The present study is aimed to investigate the electronic structure of the silver chalcogenide compounds. For Ag_2S, we have performed ab initio LMTO band calculation. For comparison, we have taken photoemission spectra of Ag_2S and Ag_2Se using a synchrotron photon source. The calculated density of states (DOS) is compared with the experimental results. The band calculation is also performed for the high temperature α-Ag_2S, and the microscopic mechanisms of the phase transition and fast ionic conduction in Ag_2S are discussed.

2. Crystal structure of β-Ag_2S, methods of calculation and experiment

The crystal structure of β-Ag_2S is shown in Fig. 1. The unit cell vectors can be expressed using the cubic vectors as [2]

$$a_\beta \simeq 1/2a_c + 1/2b_c - 1/2c_c$$

$$b_\beta \simeq a_c - b_c$$

$$c_\beta \simeq 2c_c.$$

As mentioned above, sulfur atoms form a deformed bcc lattice. There are two types of Ag atoms in the unit cell: Ag(1) is located near the octahedral 6(b)

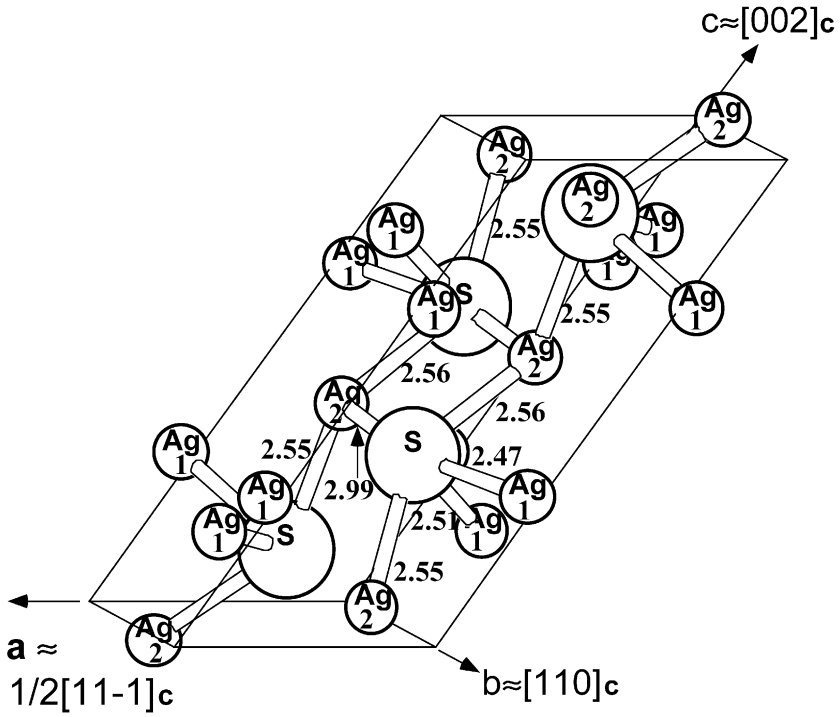

Fig. 1. Schematic drawing of the structure of β-Ag_2S (acanthite) (2). The atomic distances and the relation to the cubic cell are also shown.

site of the sulfur lattice with two sulfur atoms at 2.5 Å, one at 3.0 Å and two at 3.4 Å, while Ag(2) is located near the tetrahedral 12(d) site with three sulfur atoms at 2.5–2.7 Å and one at 3.0 Å (hereafter, we call the sites as O and T sites). Fig. 2 shows the Brillouin zone of β-Ag_2S. The crystal data of β-Ag_2S are summarized in Table 1.

The band structure is calculated using the full-potential LMTO method in the framework of the local density approximation (LDA) [14]. Details of the calculation are reported elsewhere [14,15]. In order to compare with the experimental data, calculated DOS values are convoluted with a Gaussian which has a line width of 0.5 eV.

The photoemission spectra were taken using the synchrotron radiation from SOR-RING at the Institute for Solid State Physics, University of Tokyo. Details of the measurements are reported elsewhere [16,17]. Ag_2S and Ag_2Se samples were synthesized from the elements (99.999%) by direct reaction. Stoichiometric mixtures of the elements were melted in evacuated silica tubes at about 1373 K and solidified by slow coolings. The obtained crystals were checked by taking powder X-ray diffraction patterns and comparing with the ASTM data. In order to get clean surfaces, the samples were scraped in vacuo using diamond files. The photoemission data were taken at room temperature in the vacuum of 1×10^{-8} Pa. The overall energy resolution of the measurements (ΔE) was about 0.5 eV at an excitation energy of 80 eV. The absolute values of the binding energies were determined from the Fermi edge of Au metal.

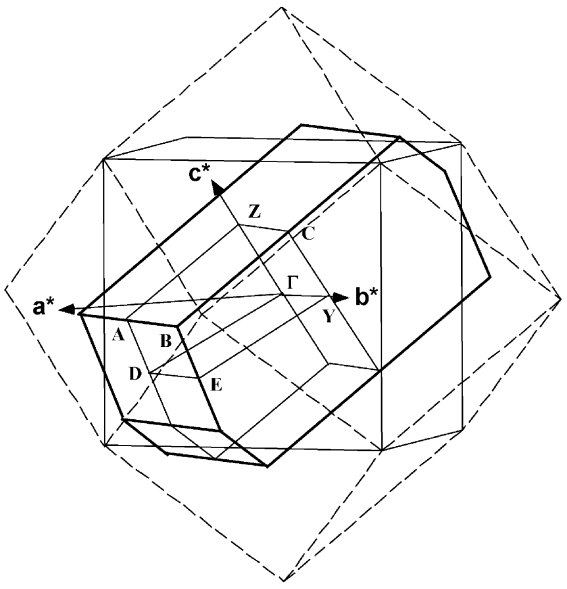

Fig. 2. Brillouin zone of β-Ag_2S (thick solid lines). The symmetry points and lines used to calculate the band structure are labelled. The Brillouin zones of the simple cubic and bcc lattices are shown by thin solid and broken lines.

Table 1
Crystal data of β-Ag_2S taken from Ref. [2]

(a) Space group, lattice parameters (in Å) and angle

Space group	*a*	*b*	*c*	*β*
$P2_1/c$	4.231	6.930	9.526	125.48°

(b) Atomic coordinates

Atom	*x*	*y*	*z*
Ag(1)	0.0712	0.0169	0.3075
Ag(2)	0.7259	0.3213	0.4362
S	0.5000	0.2383	0.1306

3. Results and discussion

3.1. The band structure and the valence band spectra

The calculated band structure of the β-Ag_2S is shown in Fig. 3. The lowest band derived from S 3s states is around −3 eV, it is well below the bands shown in Fig. 3. The main valence bands are composed of Ag 4d and S 3p states. The top of the valence bands is located at a flat band along the Γ(0,0,0)–D(0.5,0,−0.5) line. It has primarily S 3p character. The bottom of the conduction bands is at the Γ point, and has Ag s and S s–p mixed character. The calculated energy gap is 0.63 eV. From the optical and resistivity studies, the energy gap is reported as 1.2 eV [13]. This discrepancy may be attributed to drawback of the LDA which tends to underestimate energy gaps. The calculated DOS is shown in Fig. 4. The result is in good agreement with that of LMTO-ASA calculation reported by Barman et al. [18]. It may be worth to add a few features of the calculated DOS. The coordination of the Ag atoms is essentially of tetrahedral. The Ag 4d states and S 3p states form the bonding bands from 3.5 to 5 eV and the antibond-

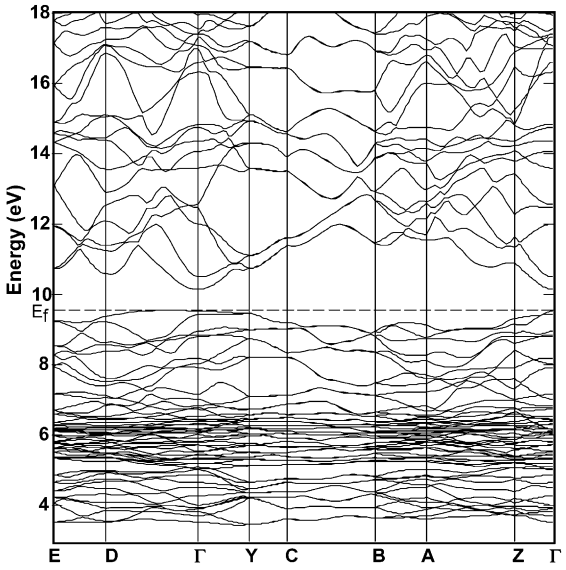

Fig. 3. Energy bands of β-Ag_2S calculated along the symmetry lines indicated in Fig. 2. The horizontal broken line show the Fermi level.

ing bands from 7 to 9.5 eV, the Ag 4d states also form the nonbonding bands from 5 to 7 eV. Since the wave functions Ag 5s and S 3p have a large overlap, the interaction between these two orbitals is rather strong. Thus, the hybridized Ag 5s states appear at the bottom of the main valence band, and the S 3p states appear in the conduction bands.

The experimental data are given in Figs. 5 and 6, which show the energy distribution curves (EDCs) of

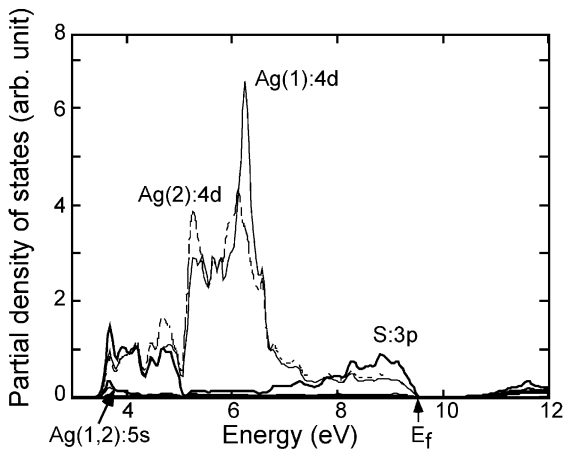

Fig. 4. Calculated partial DOS of β-Ag_2S.

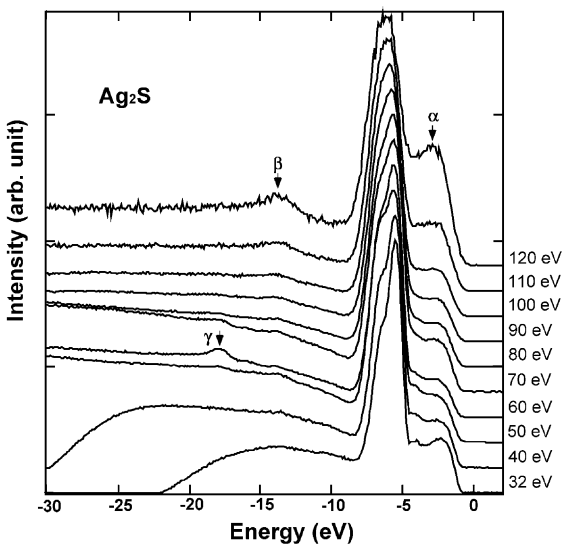

Fig. 5. Photoelectron energy distribution curves (EDCs) taken with different incident photon energies: Ag_2S. The largest peak is attributed to Ag 5d states. The spectra are normalized using the height of this peak. The peaks denoted by α, β and γ correspond to hybrid bands of Ag 4d and chalcogen p states, chalcogen s states and resonant satellites, respectively (see text).

Ag_2S and Ag_2Se measured at incident photon energies of 32–120 eV. The most prominent peak around −6eV is attributed to Ag 4d states. The spectra are normalized using the height of the Ag 4d peak. The shape of the main Ag 4d peak changes with the photon energy; at low photon energies, the shape is asymmetric with a shoulder at the high binding energy side, while at higher photon energies, the shape becomes more symmetric. This shape change is attributive the photoionization cross section minimum of Ag 4d orbitals called cooper-minimum [19]. On the high energy side of the main 4d peak, around −1 to −5 eV, a hump is observed (denoted by α in Figs. 5 and 6). In Ag_2S, the intensity of the hump increases considerably at 120 eV, the highest photon energy used here. In Ag_2Se, however, the rise is not so much. This change of the EDC profile is attributed to changes of the photoionization cross sections of chalcogen s and p states relative to that of Ag 4d (cf. Table 2). On the low energy side of the Ag 4d peak, around −8 to −11 eV, the tail has a negligible intensity in Ag_2S, while it has a larger intensity in Ag_2Se. At around −14 eV, a small peak is observed (noted by β in Figs. 5 and 6). When the incident

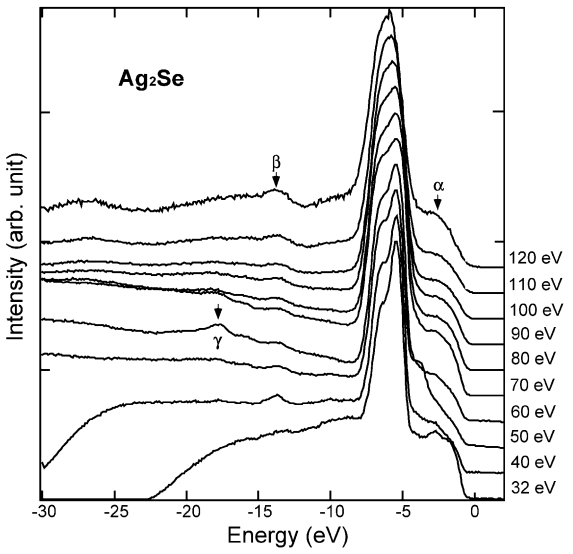

Fig. 6. Photoelectron energy distribution curves (EDCs), taken with different incident photon energies: Ag_2Se. The largest peak is attributed to Ag 5d states. The spectra are normalized using the height of this peak. The peaks denoted by α, β and γ correspond to hybrid bands of Ag 4d and chalcogen p states, chalcogen s states and resonant satellites, respectively (see text).

photon energy approaches the Ag 4p threshold of 62.9 eV, a satellite peak appeared around − 18 eV (noted by γ in Figs. 5 and 6). The satellite appears about 12 eV below the main Ag 4d-peak. It is caused by resonant two-electron excitation process in which two 4d electrons are excited simultaneously to generate photoelectron and a quasibound electron [20]. The resonant satellite is beyond the scope of this study and does not concern us.

In Fig. 7, the calculated DOS is compared with the EDC data, where the atomic cross sections in Table 2 are used as multiplication factors for the different partial DOS, and the energy scale is lined up to match the observed peak at − 6 eV. The calculated valence

Table 2
Energy dependence of the photoionization cross sections (in Mb) taken from Ref. [18]

Atom, orbit	40.8 eV	80.0 eV	132.3 eV
Ag, 4d	37.48	3.218	0.2785
S, 3s	0.4493	0.3150	0.1637
Se, 4s	0.2065	0.1810	0.1022
S, 3p	0.6029	0.6814	0.3610
Se, 4p	0.5578	0.1353	0.1005

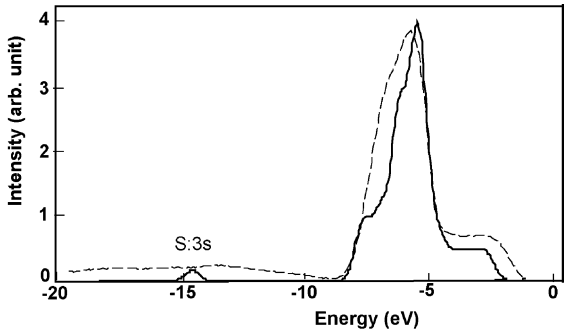

Fig. 7. Comparison of the weighted DOS (thick solid line) and the spectrum taken at 80 eV (thin dotted line). The effect of the secondary photoelectrons is subtracted, and the weights are taken from Table 2.

DOS seems to reproduce the observed EDC qualitatively. The hump at the top of the valence band is ascribed to Ag 4d and S 3p antibonding states, and the small peak at − 14 eV is ascribed to S 3s states. The profile in the low energy side of the main Ag 4d peak is, however, rather different. Around 4.5–6 eV below E_f, the calculation yields some state densities due to S 3p states, while the observed EDCs do not show any tail attributive to S 3p states. In Ag_2Se, as described above, the tail part has some intensities ascribable to Se 4p states. The reason for the discrepancies is not clear at present, since the band calculation is not performed for Ag_2Se. In order to interpret the photoemission data more precisely, including the incident energy dependence of EDCs, an elaborated theoretical treatment is needed, where not only the state densities of the initial valence band states, but also those of the available final states are taken into account.

3.2. Electronic structure of α-Ag_2S and the phase transition

Next we consider the electronic structure of the high temperature phase. As mentioned before, α-Ag_2S has a disordered structure, where Ag atoms occupy the T and O sites, only partially. The band calculation is not practical for such a partial structure. As a model that satisfies the stoichiometric condition of 2:1, we can take a cuprite lattice like Ag_2O, where Ag atoms occupy 1/4 and 3/4 along the body diagonals of the bcc lattice. However, this model is discarded since the calculated total energy of the cuprite phase is rather

high compared with that of β-Ag_2S; furthermore, cuprite structure bears little resemblance to β-Ag_2S. We take a modified bcc structures (see Fig. 8 and Table 3) where we assume that Ag atoms occupy four of the O sites, or two each of the O and T sites, or four of the T sites, periodically. In order to distinguish these from the real α-Ag_2S, we call this as α′-Ag_2S, and O type, OT type and T type, respectively. The hypothetical α′-Ag_2S has the monoclinic symmetry $P2_1$. The *c*-vector is half that of β-Ag_2S, there are two Ag and one S atoms in the asymmetric unit. It would be clear that the OT type has an Ag configuration close to that of β-Ag_2S.

The calculated total energies show that the OT type has lower energies than those of O and T types. The difference will be ascribed to the Coulomb interaction between the Ag atoms; the distance between Ag(1) and Ag(2) atoms is 2.71 Å in the OT type, while it is 2.43 Å in the O or T type. This change of Ag–Ag atomic distance makes the calculated band gap open in the OT type, while close it in O and T types (see Fig. 9). In the latter two types, the conduction band bottom is found to be derived from Ag 5s states, while in the OT type, it is derived from Ag 5s–4d and S 3p mixed states. The total energy of the β-phase is slightly lower than that of the OT type, 0.09 eV/chemical unit. We can consider the atomic coordination from the view point of resonance by Pauling [21]. There are two Ag coordinations O and T, which behave as canonical structures having almost equal energies. A linear combination of these two states can have a lower energy than these two states. Thus, the resulting coordination has the character of the both O and T states, as shown in Fig. 8(c) and (d).

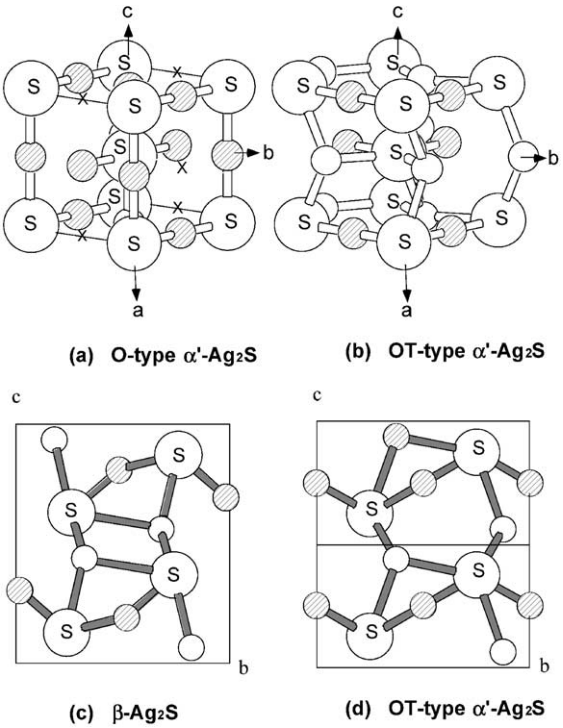

Fig. 8. Schematic drawing of the hypothetical structures of α′-Ag_2S (a) O type and (b) OT type. Open and hatched circles show Ag atoms at T:12(d) and O:6(b) sites. In a, note the periodic array of Ag vacancies at the O sites denoted by crosses. Comparison of the two structures, (c) β-Ag_2S and (d) OT-type α′-Ag_2S, projection along the *a*-axis. In c, note that the Ag coordinations have the characters of both T and O types (see text).

Table 3
Crystal data of the hypothetical α′-Ag_2S

(a) Space group, lattice parameters (in Å) and angle

Space group	*a*	*b*	*c*	*β*
$P2_1$	4.20	6.86	9.70	125.26°

(b1) Atomic coordinates (O type)

Atom	*x*	*y*	*z*
Ag(1)	0.000	0.000	0.500
Ag(2)	0.500	0.250	0.750
S	0.500	0.250	0.250

(b2) Atomic coordinates (OT type)

Atom	*x*	*y*	*z*
Ag(1)	0.000	0.000	0.500
Ag(2)	0.750	0.375	0.875
S	0.500	0.250	0.250

(b3) Atomic coordinates (T type)

Atom	*x*	*y*	*z*
Ag(1)	0.250	0.125	0.625
Ag(2)	0.750	0.375	0.875
S	0.500	0.250	0.125

The nonmetal–metal nature of the α–β phase transition in Ag_2S has been investigated by several researchers. At the transition, the electrical conductivity increases nearly three orders of magnitude [12,13]. The UPS data show, however, no detectable change of DOS near the E_f region [18]. The band gap is reported to decrease from 1.2 to 0.4 eV (13). We

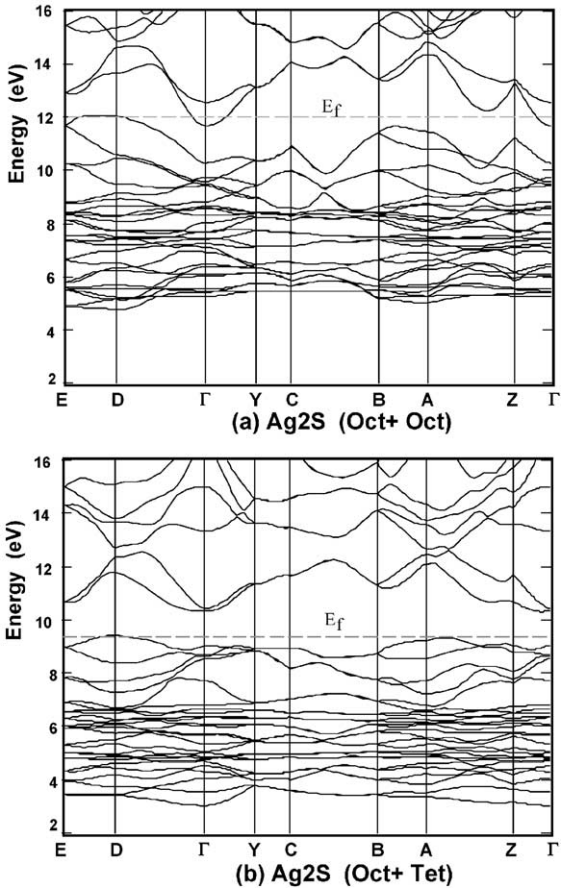

Fig. 9. Energy bands in the hypothetical two structures of α′-Ag_2S, with Ag coordinations: (a) octahedral, and (b) octahedral and trahedral. The horizontal broken line show the Fermi level. Note that the band gap is closed in a, but open in b, and that the band energy is higher in a.

consider that the rise of the electrical conductivity is attributive to the partial local structures belonging to the O and T types, where the band gap disappears. However, the ratio that O and T type structures occur is not so much as to influence on the total DOS near the E_f region.

Ag_2S crystal is reported to show a premonition of the phase transition, the twin structure becomes minute as the transition temperature is approached [2]. The crystal first adjusts its monoclinic β-angle to that of the hypothetical α′-Ag_2S 125.26° (the angle between the [1,1,−1] and [0,0,1] axes of the cubic cell). In the next step, the crystal mimics cubic symmetry by twinning. The high temperature phase is composed of an aggregate of microscopic acanthite twins. As the temperature increases, the atomic arrangement deviates gradually from that of β-Ag_2S and approach more symmetric cubic structure.

3.3. Fast ionic paths in α-Ag_2S

Lastly, we discuss the ionic transport in α-Ag_2S. Fig. 10 shows the total energy of α′-Ag_2S plotted against the Ag coordinates. We can see that when Ag(1) atoms occupy O sites, Ag(2) atoms can move between a pair of T sites quite easily, and that when Ag(1) atoms occupy T sites, Ag(2) atoms can move around O sites also easily. The figures are indicating the fast-ionic paths in the cubic phase. Neutron diffraction [4] and molecular dynamic studies [11] showed that as the temperature increases, the Ag population at O sites decreases and the conduction path changes from T–O–T to T–24(h)–T. Fig. 10

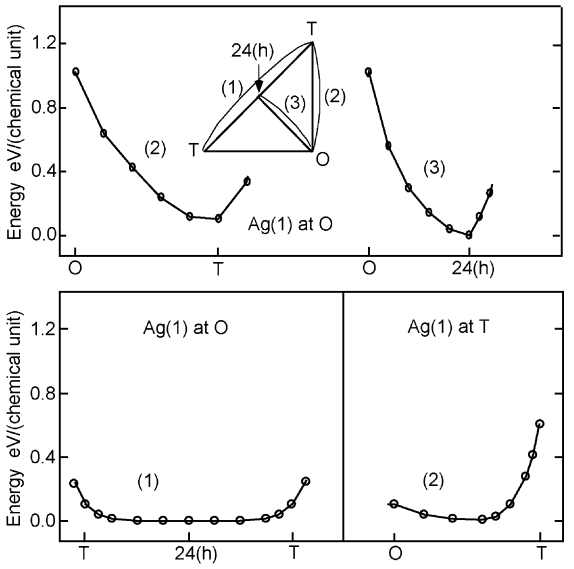

Fig. 10. Calculated total energy in the hypothetical α′-Ag_2S plotted as functions of the Ag coordinates. The triangle inserted in the upper part figure shows O:6(b), T:12(d) and 24(h) sites of the bcc lattice. The numbers in parentheses show the paths where the calculations are done. In upper and lower left side figures, Ag(1) is fixed at O sites, while in the lower right figure, Ag(1) is fixed at T sites. The horizontal axes show the positions of Ag(2) atom, and the vertical axes show relative energies in eV/chemical unit.

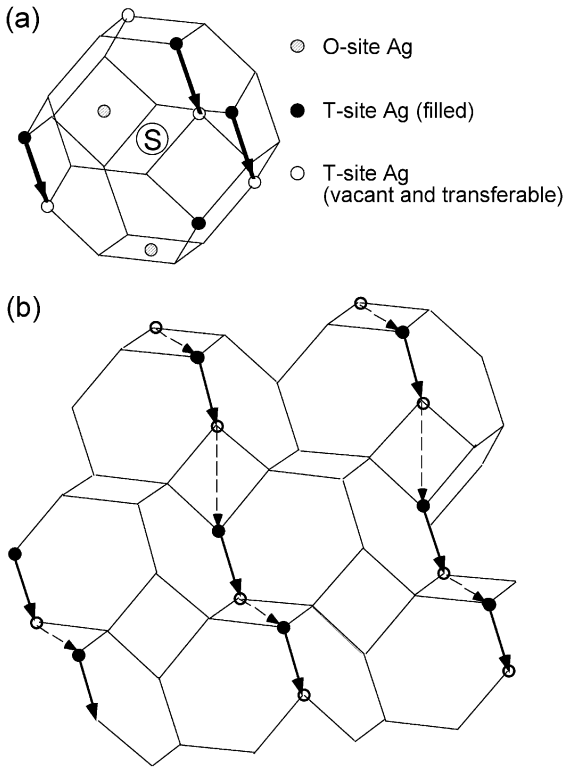

Fig. 11. (a) Schematic drawing of Ag coordination around a sulfur atom. The cubo-octahedrons show T:12(d) sites in the bcc lattice. (b) A model of the cooperative ionic transport in α-Ag_2S. Filled circles show T sites filled with Ag atoms and open circles show transferable vacant sites. For clarity, S atoms and Ag atoms at O sites are omitted. As seen in Fig. 7, Ag atoms are easy to move from the filled sites to vacant circles connected by arrows. The motion induces another transfer through the path represented by dotted arrow directed along the [100] or [010] axis.

shows that the 24(h)−T−24(h)−T channel has a very low activation energy of 0.1 eV/chemical unit. The activation energy of the Ag transport is reported as 0.1 eV. [12]. We can see in Fig. 10 that the T site is not the energy minimum point but a saddle point. This corresponds to the fact that the ionic distribution at the T site is represented by asymmetric anharmonic thermal vibrations which have four lobes along the <110> axes. Lastly, we note that in this calculation the atomic displacements are assumed to occur cooperatively. In silver chalcogenide compounds, Yokota [22] first proposed cooperative ionic transport, in order to explain small Haven's ratio of the diffusion coefficients derived from tracer and ionic conductivity measurements, and named it as caterpillar mechanism. Fig. 11 shows a model for cooperative ionic transport in Ag_2S. The diffuse X-ray and neutron scatterings by Cava et al. [8,9] also have proved strongly correlated ionic transport in α-Ag_2S.

In summary, using photoemission, we have studied the electronic structure of the silver chalcogenide compounds Ag_2S and Ag_2Se. For Ag_2S, the result is compared with the LMTO band calculation and qualitative feature of the EDCs has been reproduced. The mechanisms of the structural phase transition and superionic conduction are discussed. For Ag_2Se, the band calculation is not performed due to the lack of detailed crystal data.

Acknowledgements

The experiments were done under the Cooperative Research program of the Institute for Solid State Physics University of Tokyo. The authors thank the staff of SOR-RING the Institute for Solid State Physics, University of Tokyo, for excellent support. This work was partially supported by the Uchida Energy Science Promotion Foundation.

References

[1] A.J. Frueh, Z. Kristallogr. 110 (1958) 136.
[2] R. Sadanaga, S. Sueno, Mineral. J. Jpn. 5 (1967) 124.
[3] P. Rahlfs, Z. Phys. Chem., B 31 (1935) 157.
[4] R.J. Cava, F. Reidinger, B.J. Wuensh, J. Solid State Chem. 31 (1980) 69.
[5] G.A. Wiegers, Am. Mineral. 56 (1971) 1882.
[6] R. De Ridder, S. Amelinckx, Phys. Status Solidi, A 18 (1973) 99.
[7] Y. Tsuchiya, S. Tamaki, Y. Waseda, J.M. Toguri, J. Phys. C 11 (1978) 751.
[8] R.J. Cava, D.B. McWhan, Phys. Rev. Lett. 45 (1980) 2046.
[9] B.H. Grier, S.M. Shapiro, R.J. Cava, Phys. Rev., B 29 (1984) 3810.
[10] S. Ihara, K. Suzuki, J. Phys. Soc. Jpn. 53 (1984) 3081.
[11] J.R. Ray, P. Vashishta, J. Chem. Phys. 90 (1989) 6580.
[12] S. Miyatani, J. Phys. Soc. Jpn. 10 (1955) 786.
[13] P. Junod, H. Hediger, B. Kilchor, J. Wullschleger, Philos. Mag. 36 (1977) 941.
[14] S.V. Savrasov, Phys. Rev., B 54 (1996) 16470.
[15] S. Kashida, N. Watanabe, T. Hasegawa, H. Iida, M. Mori, Solid State Ionics 148 (2002) 193.
[16] A. Kakizaki, H. Sugawara, I. Nagakura, T. Ishii, J. Phys. Soc. Jpn. 49 (1980) 2183.

[17] S. Kashida, T. Saito, M. Mori, Y. Tezuka, S. Shin, J. Phys., Condens. Matter 9 (1997) 10271.
[18] S.R. Barman, N. Shanthi, A.K. Shukla, D.D. Sarma, Phys. Rev., B 53 (1996) 3746.
[19] J.J. Yeh, I. Lindau, At. Data Nucl. Data Tables 32 (1985) 1.
[20] M.R. Thuler, R.L. Benbow, Z. Hurych, Phys. Rev., B 26 (1982) 669.
[21] L. Pauling, The Nature of the Chemical Bond, 3rd ed., Cornell Univ. Press, Ithaca, NY, 1960.
[22] I. Yokota, J. Phys. Soc. Jpn. 21 (1966) 420.